Performance of Electrospray Thrusters

IEPC-2009-242

Presented at the 31st International Electric Propulsion Conference,
University of Michigan • Ann Arbor, Michigan • USA
September 20 – 24, 2009

John K. Ziemer*
Jet Propulsion Laboratory, California Institute of Technology, Pasadena, CA, 91109, USA

Electrospray thrusters are a class of electrostatic electric propulsion experiencing renewed growth in research and application. In these devices high electric fields (~10^9 V/m) are applied to a conductive liquid propellant at micron-scale emission sites, producing and accelerating charged droplets, clusters, or ions without the use of a plasma discharge. Often labeled as colloid or field emission electric propulsion (FEEP) thrusters, emission current and thrust values are typically on the order of microamps and micronewtons per emission site. Propellants have included molten metals such as cesium, indium and rubidium, semi-conductive liquid mixtures, and more recently room temperature liquid salts (RTLS), often termed ionic liquids. With just a few emitters working in parallel, electrosprays have demonstrated the capability to provide sub-micronewton level thrust precision, resolution, and noise. These performance characteristics make them an ideal choice to meet the stringent requirements for precision formation flying and drag-free missions such as the Laser Interferometer Space Antenna (LISA), designed to detect gravity waves. With many more emitters working in parallel, these devices can be scaled up in thrust to mN levels while maintaining high efficiency. Direct thrust stand measurements have demonstrated >80% efficiency at specific impulse values from 100-10000 s for single and multiple (but <10) emitter thrusters. We present a performance model for electrospray thrusters and use thrust measurements to verify these models. The purpose of this paper is to provide the electric propulsion community with a better understanding of electrospray propulsion and validated performance models that can be used to predict thruster performance.

Nomenclature

C_1	=	Colloid thrust coefficient
C_{eff}	=	Thrust efficiency coefficient
I	=	Total current supplied to the emitter array
I_{emit}	=	Current actually emitted by a single emitter that passes through the electrodes and produces thrust
I_{grid}	=	Current intercepted by the electrodes
I_n	=	Current emitted by a single electrospray emission site
m	=	Mass of a single particle (droplet, cluster, ion, etc.)
$\dot{m}$	=	Total mass flow rate supplied to the emitter array
$\dot{m}_{emit}$	=	Mass flow rate actually emitted by a single emitter that passes through the electrodes
$\dot{m}_n$	=	Mass flow rate supplied to and used in a single electrospray
N	=	Number of emitters in an array
$P_{elecdisp}$	=	Power dissipated by the electronics from supplying power to the other subsystems
P_{heater}	=	Power supplied to any heater subsystem not included in the PMS power
P_{input}	=	Total input power to the electrospray propulsion system

* Senior Engineer, Electric Propulsion Group, email: John.K.Ziemer@jpl.nasa.gov.

P_{PMS} = Power supplied to the propellant management system (PMS)
P_{neut} = Power supplied to the cathode neutralizer
q = Charge on a single particle (droplet, cluster, ion, etc.)
$<q/m>$ = Average charge-to-mass ratio in an electrospray
T = Total thrust produced by the entire emitter array
T_{emit} = Thrust produced by a single emitter
T_{ideal} = Maximum thrust produced by a single emitter
T_{linear} = Thrust produced by a single emitter with a "linear" exhaust (no beam spreading)
$\bar{u}_e$ = Mass averaged exhaust velocity
u_{emax} = Maximum exhaust velocity
u_{ex} = Expected exhaust velocity
V_{beam} = Beam voltage (emitter potential with respect to ground)
α = Droplet mass and current parameter
η = Total system efficiency
η_{curr} = Current supply efficiency
η_{grid} = Grid interception efficiency
η_{ion} = Charged particle production efficiency
$\eta_{q/m}$ = Charge-to-mass ratio distribution efficiency
η_{spread} = Beam spreading efficiency
$\eta_{thruster}$ = Thruster efficiency
η_{util} = Propellant utilization efficiency
θ_h = Exhaust beam half-angle enclosing 95% of the total emitted current

I. Introduction

ELECTROSPRAY propulsion has been studied since the early sixties through research into colloid thrusters and liquid metal ion sources (see reviews in Refs. 1 and 2). An electrospray produces thrust by generating and accelerating charged particles (droplets, clusters, ions) with electrostatic fields. The charged particles are created by applying an electric field of ~10^9 V/m to a conductive liquid propellant at an emitter tip. A balance between the applied field and surface tension forces creates a Taylor cone emission site and an electrospray. Depending on the physical properties of the propellant (conductivity, surface tension, dielectric strength, etc.), the applied field strength, the flow rate to the emitter, and the physical geometry of the emitter, a stable electrospray can produce between 100 nA – 100 μA of current with applied voltages of 1000 – 10000V. This leads to a 10000X factor in power processing capability for an individual emitter with power levels between 0.1 mW – 1 W per emitter. Thrust can be as high as 10 μN per emitter with thrust-to-power ratios of over 100 mN/kW, rivaling higher-power ion and Hall thruster performance. In the late 1960's and early 1970's colloid thrusters with arrays of 100's and even 1000's of emitters were developed and tested for 1000's of hours, but using low conductivity fluids requiring voltages >10 kV to reach specific impulse values that could compete with discharge ion thrusters. Research into using electrosprays for propulsion then paused while the main focus was kept on conventional ion thrusters.

Electrospray propulsion research and flight systems development picked up again in the early 1990's and continues on today, focusing on precision propulsion applications. Two types of electrospray propulsion will be demonstrated on the LISA Pathfinder Mission: Colloid Micro-Newton Thrusters (CMNTs) developed by Busek Co.[3,4] and NASA JPL[5], and Cesium Slit-FEEP thrusters developed By Alta, Galileo Avionica, Astrium and ESA[6]. In the future, larger arrays with 10^2 - 10^4 emission sites could produce multi-millinewton level thrust over a wide range of specific impulse values (100 - 10000s) at greater than 80% thrust efficiency, using less than 1 kW of power. Ideal for small-sat missions, these devices can also be scaled up to primary propulsion applications.

In this paper we will describe the basic performance scaling relationships for electrospray thrusters. Loss mechanisms such as ion production energy, propellant utilization efficiency, mixed species production, and beam divergence will be discussed along with direct thrust measurements from both colloid and FEEP electrospray thrusters. We will show that scaling relationships derived from basic physical principles have been verified by thrust, specific impulse, and exhaust beam energy and charge-to-mass ratio measurements made by the author and found in the literature. Electrospray thrusters can operate in a charged droplet, cluster, ion, and frequently a mixed mode of emission. Each mode has its own performance characteristics, which will be discussed in this paper. On a single emitter basis, the predicted and measured performance of these electrospray devices can surpass any other available electric propulsion system.

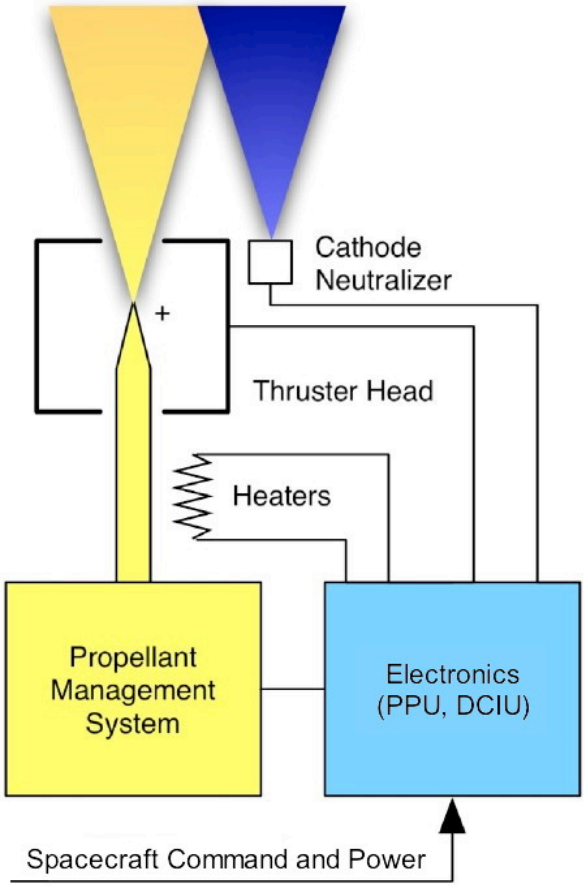

Figure 1. Electrospray propulsion system-level block diagram.

II. Description of Electrospray Propulsion Devices

An electrospray propulsion system uses a conductive liquid propellant with electrodes that create and accelerate charged particles to high velocities. In this section, we describe each of its subsystems and the basic performance relations including thrust and exhaust velocity in relation to key parameters such as beam voltage. We also discuss the various electrode geometries that can be found in modern devices.

A. System-Level Description

An electrospray propulsion system includes the following subsystems, as shown in Figure 1: thruster head, cathode neutralizer, propellant management system (PMS), and electronics. In some cases a heater may also be required to liquefy the propellant or maintain physical properties at constant levels, but is often part of the thruster head or the PMS subsystems.

The thruster head includes the emitters, electrodes, electrode isolator, and any manifold or other propellant feed element that accepts the output from the PMS and distributes the propellant to the individual emitters. Again, the thruster head may also include a heater, but does not include, in general, any active flow control device unless the subsystems are much more closely integrated. The thruster head and manifold may have passive flow control, typically provided by using small, ~100 μm sized channels to distribute the propellant evenly between the emitters. The emitters themselves can have a significant hydraulic resistance, again helping to distribute the flow more evenly.

The cathode neutralizer provides the necessary electrons to balance the charge emitted by the thruster head. Typically the cathode is a solid-state device, either a heated filament of some kind or a low-work function material with it's own set of electrodes. MEMS Spindt type and carbon-nanotube cathodes have also been tested and developed for this application [7]. In a unique approach, the neutralizer itself could also be an electrospray producing *negatively* charged particles that may also generate a significant amount of thrust. In that case, the neutralizer would also require its own PMS since the two conductive-propellant feed-systems must be kept at different potentials. This approach has both advantages and disadvantages that will not be discussed any further in this paper since it is such a special case.

The propellant management system (PMS) consists of the propellant tank, plumbing, valves, and any active control of the propellant flow rate. The PMS may also contain heaters (in some cases to liquefy the propellant) and some method of pressurizing or feeding the propellant. In some cases, the PMS can be completely or partially passive using only capillary action with temperature as the only control. Part, if not all, of the PMS must be kept at the same voltage as the emitter since the propellant is a conductive liquid. Electrical isolation between the propellant storage tank and thruster head is very difficult. In many designs, the PMS is integrated very closely with the thruster head to save mass and volume.

The electronics typically consist of at least two units: the digital control and interface unit (DCIU) that takes in the spacecraft provided power, command, and telemetry interface, and the power processing unit (PPU) that converts the low voltages provided by the DCIU (or spacecraft directly) to the high voltages necessary for operation. There can be multiple high voltage converters in a PPU supplying power to the electrodes, certain PMS components that require high voltage, and the cathode neutralizer. The DCIU may also supply lower voltages (typically <28V) to various PMS components and heaters. If multiple thrusters are to be operating at once, the DCIU can be designed to operate multiple PPUs, one for each thruster head or more if redundant systems are required.

B. Thrust Relations

Electrospray propulsion devices produce thrust by accelerating charged particles (droplets, clusters, ions, or combinations of them) with an applied electrostatic field. The maximum exhaust velocity, $u_{e\max}$, of a single particle with charge, q, and mass, m, along the intended thrust vector can be derived from conservation of energy,

$$u_{e\max} = \sqrt{2\frac{q}{m}V_{beam}}, \tag{1}$$

where V_{beam} is the beam voltage (emitter potential with respect to ground). From this relation the exhaust velocity can be seen to vary with the square root of the applied voltage and charge-to-mass ratio. The charge-to-mass ratio is one of the key performance parameters of an electrospray, which can vary except in pure ion emission mode. However, to estimate a maximum bound for thrust, we will assume there are no losses to the grids, beam spreading, or propellant inefficiencies, and the average charge-to-mass ratio, $<q/m>$, is related to the emitted mass flow rate, $\dot{m}_{emit}$, and emitted current I_{emit} ratio. For our analysis, we will also assume the average charge-to-mass ratio is uniform over the entire exhaust beam, leading us to the useful identity that the mass flow rate and current supplied to a single emission site, $\dot{m}_n$ and I_n, respectively, have the same ratio,

$$\left\langle \frac{q}{m} \right\rangle = \frac{I_{emit}}{\dot{m}_{emit}} = \frac{I_n}{\dot{m}_n}. \tag{2}$$

Considering only charged particles contribute to the thrust, the maximum thrust from a single emitter, T_{ideal}, is then the maximum exhaust velocity multiplied by the emitted mass flow rate (and using Eq. (2)),

$$T_{ideal} = I_n\sqrt{2\left\langle \frac{m}{q} \right\rangle V_{beam}}. \tag{3}$$

Using this relation, the ratio of the ideal thrust produced by an emitter to the power going into the emitter would not depend explicitly on the emitted current and is inversely proportional to the maximum exhaust velocity. That is, as the exhaust velocity is increased, thrust is reduced and vice versa. For the thrust-to-power ratio, the two key performance parameters are only the charge-to-mass ratio and applied beam voltage. In practice the charge-to-mass ratio is indeed a function of the operating current, extraction voltage, and temperature through the physical properties of the propellant. Additional performance parameters and relations, including efficiency, and more realistic loss-terms will be included and described in Section III.

C. Emitter and Electrode Geometries

There are three conventional electrode geometries for a single emitter: needle, capillary, and slit, as shown in Figure 2. We will now briefly describe each.

In the needle geometry, propellant wicks up the outside of the emitter to the base of the Taylor Cone. The flow rate is governed by emitter surface conditions and wetting characteristics. Multiple needles must be used to reach higher thrust levels to prevent wide exhaust beams (space charge at emitter tips determines beam divergence). This is a very common geometry for FEEP thrusters, and this geometry is still in heavy use today.

In the capillary geometry, propellant either wicks up in the inside of the emitter through capillary action or can be forced to the emitter tip by a controlled, pressurized source. The Taylor Cone size is driven by capillary diameter; however, multiple emission sites can be generated on the rim of the emitter with high fields or low flow rates. Multiple or larger capillary emitters must be used to reach higher thrust levels. This is a very common geometry used on multiple colloid thruster designs. FEEPs have also employed this approach with a passive capillary-driven system.

In the slit design, propellant either wicks up the inside of the emitter through capillary action or can be forced to the emitter tip by a controlled, pressurized source. The slit can be linear, as in the Cs-FEEP design, or as the gap between two annular rings. Multiple Taylor Cone emission sites form along the length of the slit with a wavelength that depends on the slit width, propellant physical properties, and the applied electric field strength; however, if left

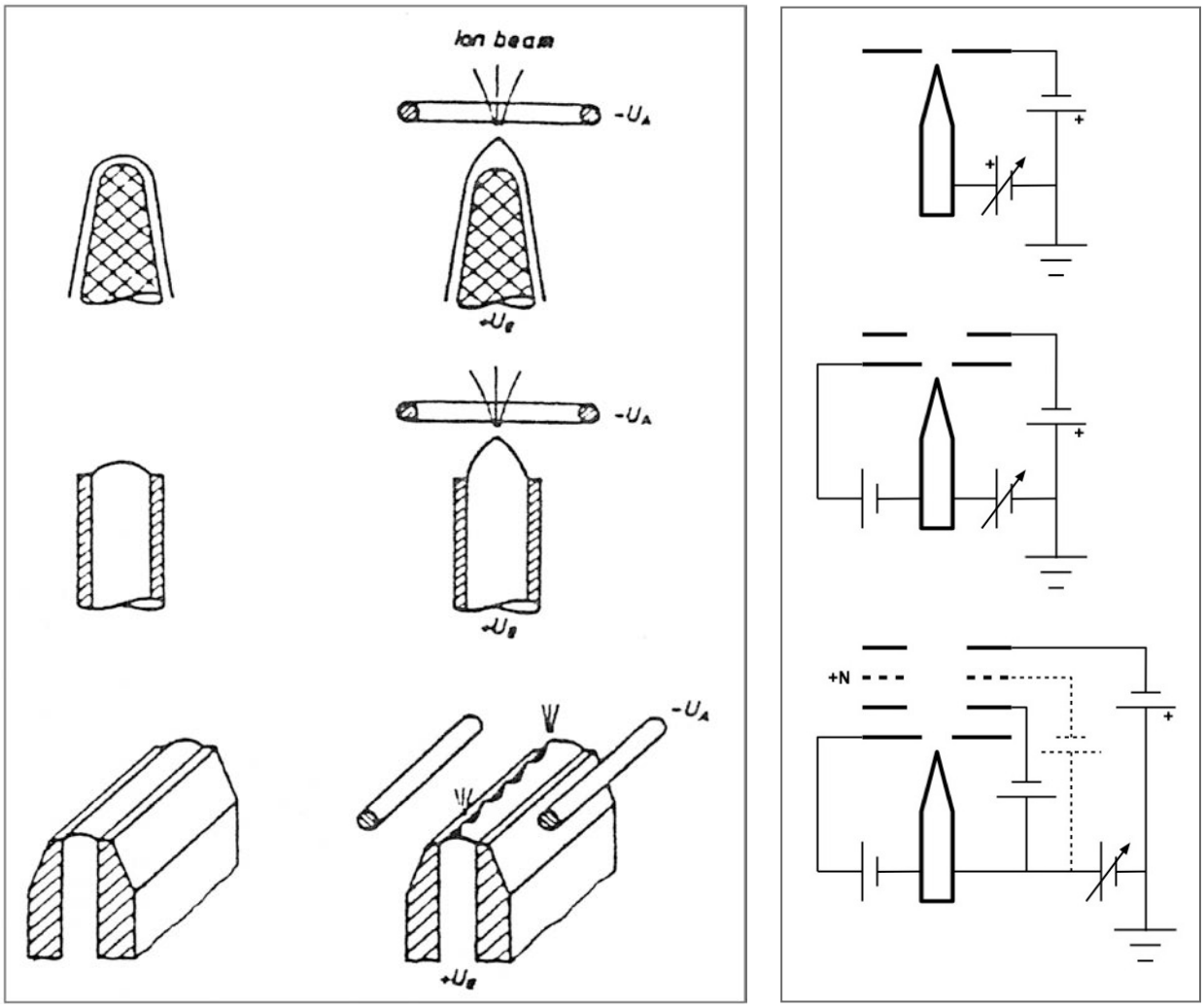

Figure 2. Electrospray electrode geometries including three common emitter styles (left drawing, taken from Mitterauer, 1987 [2]) and downstream electrode geometries (right schematic).

to their own, the emission sites are not typically uniform in practice. Thrust level is determined by slit length, but linear slits (as apposed to circular) can have large beam divergence issues perpendicular to the slit length.

Figure 2 also shows three different but common electrode geometries, increasing in complexity: the single grid system, the two-grid system, and the "N" grid or multi-grid approach.

In the single grid system, the emitter is biased positively and flow rate is controlled to produce ions or positively charged droplets. The extractor is biased negatively (usually at constant voltage) to repel back-streaming electrons from the ambient space plasma or testing environment. This is an appealing and simple geometry, but notice that the extraction field is variable along with total acceleration voltage. Still, this design has been used in flight FEEP thrusters and simple laboratory studies.

In the two-grid system the emitter is biased positively or negatively and controlled to produce ions or charged droplets in either polarity. The extractor is set with a fixed potential with respect to the emitter to produce positively or negatively charged particles at a fixed voltage. The accelerator is biased negatively (usually at constant voltage) to repel back-streaming electrons. This allows a stable and constant extraction process while the full beam potential can be varied to control thrust and Isp. This is a very common approach used in many colloid thrusters, include those produced for ST7.

The multi-grid system is similar to the two-grid system, but an additional grid is added to help focus or decelerate the beam. Complexity improves performance but adds risk of additional paths for shorting and alignment complexity. Still, with decent electrostatic modeling tools, the electrodes can be optimized.

III. Electrospray Propulsion Performance Model

In this section we will present a more detailed account of the electrospray propulsion system performance by breaking down the efficiency of the system. Specifically, we will focus on the thruster efficiency including loss mechanisms for propellant utilization, current leakage paths, ionization costs, grid impingement, exhaust beam spreading, and having a non-singular charge-to-mass distribution. We will then look at different modes of operation in terms of the average charge-to-mass ratio of the exhaust beam, producing droplets, ions, or a mixture of both.

A. General Efficiency Description

We begin to break down the efficiency of an electrospray propulsion system by separating out the power supplied to the thruster from the power required by the DCIU, PPU, PMS, and cathode neutralizer to run the system. While these terms are significant in the fraction of power they consume, they are relatively straightforward to determine and do not depend directly on the key electrospray characteristics. The overall system efficiency, η, and total input power to the system, P_{input}, is broken down as follows:

$$\eta = \eta_{thruster}\left(\frac{V_{beam}I}{P_{input}}\right), \tag{4}$$

$$P_{input} = V_{beam}I + P_{elecdisp} + P_{heater} + P_{PMS} + P_{neut}, \tag{5}$$

where $\eta_{thruster}$ is the thruster efficiency, I is the total current supplied to all the emitters in the thruster head, and $P_{elecdisp}$ is the power dissipated by the thruster electronics from producing the operational voltages to all subsystems, including any power that doesn't go into the thruster ($V_{beam}I_{tot}$), heater (P_{heater}), PMS (P_{PMS}), and neutralizer (P_{neut}). We will assume that any power going into the heater, PMS, and neutralizer does not contribute to producing thrust. In some cases, the power supplied to the heater or PMS can indeed impact performance through changing the physical properties of the propellant, but we will still consider this an overall loss term. Obviously, the case where a negative polarity electrospray is used as a neutralizer would have to be examined separately.

With T as the total thrust produced by all the emitters and $\dot{m}$ as the total mass flow rate supplied to all the emitters, the thruster efficiency can be broken down further into six terms,

$$\eta_{thruster} = \frac{T^2}{2\dot{m}V_{beam}I} = \eta_{util}\eta_{curr}\eta_{ion}\eta_{grid}\eta_{spread}\eta_{q/m}. \tag{6}$$

The six efficiency terms are related to propellant utilization, η_{util}, current supply efficiency, η_{curr}, charged particle production, η_{ion}, grid current interception, η_{grid}, beam spreading, η_{spread}, and the distribution of charge-to-mass ratios of the various charged species produced by the electrospray, $\eta_{q/m}$. We will now describe each efficiency term and in following subsections focus on the charge-to-mass ratio distribution, which depends strongly on the primary emission mode: droplet or ion.

1. Propellant Utilization Efficiency

In some cases the propellant supplied to the emitter is not completely used by the thrust-producing electrospray. Propellant may be able to evaporate before being emitted or slightly charged particles may be emitted away from the emitter tip (i.e. from an externally wetted surface) without producing a significant amount of thrust (often captured again inside the thruster head without being able to be reused). The propellant utilization efficiency, η_{util}, is then simply the ratio of the mass flow rate in an individual electrospray, $\dot{m}_n$, to the supplied mass flow rate, and we assume there is a uniform flow to all N emitters,

$$\eta_{util} = \frac{\dot{m}_n N}{\dot{m}}, \tag{7}$$

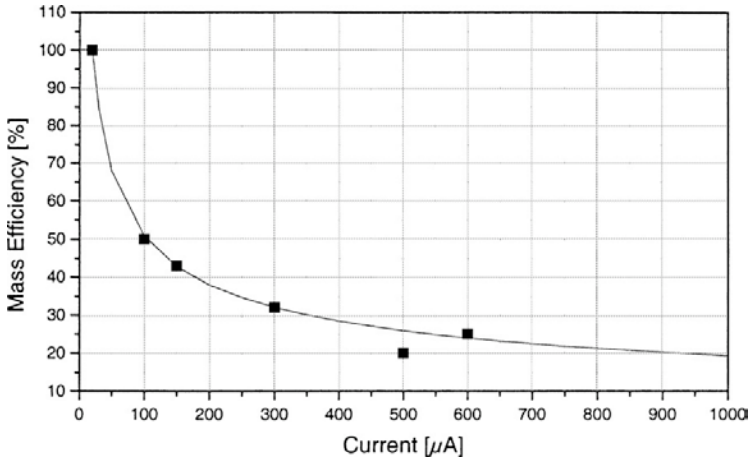

Figure 3. Propellant mass utilization efficiency as a function of emitted current for a single Indium FEEP needle emitter. Taken from Tajmar, Ref. [8].

This efficiency can be measured by operating an emission site for long periods with constant current and voltage and measuring the amount of propellant mass the emitter has used. An example of a propellant utilization measurement in an Indium Needle-FEEP thruster is given in Figure 3, taken from Ref. 8. This efficiency can reach nearly unity for other types of feed systems with internally wetted capillary emitters using very low vapor propellants. For the Indium FEEP, the propellant utilization efficiency decreases rapidly for >20 μA due to the creation of microdroplets emitted from the side of the needle. While these droplets have not been observed to increase thrust, they can have a significant impact on the efficiency.

2. Current Supply Efficiency

As an electrospray thruster operates, frequently parallel current paths can form as propellant condenses on the electrode isolators. While this is not true for all electrospray types or propellants, it occurs routinely in others and can impact the overall efficiency significantly. This efficiency can also change over time, decreasing as operating hours increase with thickening layers of propellant on the isolator, or decreasing as either heaters or the power dissipated by running current through the film helps to evaporate it or change it to a lower conductivity state. The current supply efficiency, η_{util}, is then defined as the ratio of the total current emitted by all the electrospray emission sites to the total current supplied to the thruster head electrodes,

$$\eta_{curr} = \frac{I_n N}{I}, \tag{8}$$

where I_n is the electrospray current produced by each emission site, again assumed to be uniform over the entire emitter array. This efficiency can be determined by measuring the current produced by the emitter (provided that the electrodes do not intercept any current) via a beam target, and comparing the total array emitted current with the current supplied to the full emitter array. In most cases, especially at the beginning of the thruster life, this efficiency should be near unity. However, if propellant begins to condense and form a conductive film on the electrode isolator, a parallel current path can develop, and the power dissipation can eventually become significant. Note that electrode isolator impedance values must be kept > 10^9 Ohm for typical operating conditions (10 kV/10 μA) for this efficiency to remain high.

3. Charged Particle Production Efficiency

Frequently the charged particles produced by the electrospray do not have the same energy as the emitter potential after they have been extracted and accelerated. The Taylor cone jet can actually have a significant voltage drop, V_{tc}, between the emitter electrode and the emission site. In some cases, different species are emitted from different places on the Taylor cone as well, which leads to each species having a characteristic energy. This energy loss can be determined by retarding potential analyzer measurements in the plume, comparing the energy of the emitted particles with the emitter potential. The charged particle production efficiency, η_{ion}, is defined in terms of the Taylor cone voltage loss, V_{tc}, as follows,

$$\eta_{ion} = 1 - \frac{V_{tc}}{V_{beam}}. \tag{9}$$

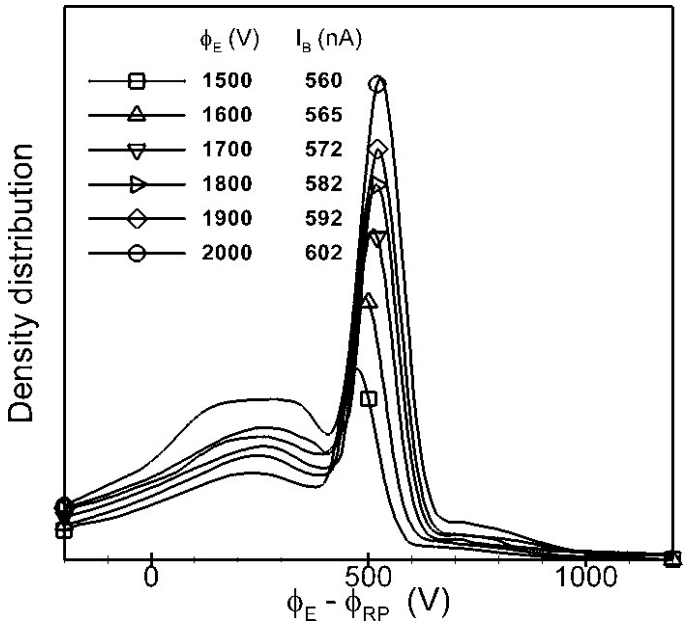

Figure 4. Retarding potential measurements along the axis of an EMI-Im electrospray, taken from Gamero, Ref. 9. Emitter extraction voltage and flow rate are varied to create the curves, but the main energy peak remains just under 500 V below the emitter.

Retarding potential measurements made by Gamero in Ref. 9 are shown in Figure 4. These measurements were taken along the axis at different flow rates and extraction voltages (all producing stable electrosprays), yet the peak of the particle energy is always nearly 500V below the emitter potential. Other particles appear to have slightly more energy, which may bring the average V_{tc} value for this data set slightly below 500V, which agrees well with thrust stand measurements shown in Section IV-A. This efficiency term is one of the most significant, and drives these devices to operate at higher voltages for higher performance. The Taylor cone voltage drop depends mainly on the physical properties of the propellant and needs to be measured for each electrospray to evaluate the performance.

4. Grid Current Interception Efficiency

When operating at lower voltages or at high emission currents, space charge density at the emission tip is high enough to cause significant spreading of the charged particles in the exhaust beam. At some point the exhaust beam can spread enough to intercept one or more of the electrodes. This reduces the emitted current to $I_{emit} = I_n - I_{grid}$, where I_{grid} is the current to the electrodes. The grid current interception efficiency, η_{grid}, can now be defined as,

$$\eta_{grid} = \left(\frac{I_{emit}}{I_n}\right)^2 = \left(1 - \frac{I_{grid}}{I_n}\right)^2. \tag{10}$$

With proper design, this efficiency should be unity. As long as the total current provided to the entire array is well distributed among the emission sites and there are enough emission sites to prevent high current densities, this efficiency is usually one of the highest, almost always near unity.

5. Beam Spreading Efficiency

Due to the very small dimensions of the emission site, the charged particle trajectories produced by electrosprays tend to be divergent from its origin. Electrode design can do a great deal to shape the exhaust beam back to nearly parallel, but extra electrodes are generally required to focus the beam, which increases complexity and may reduce reliability. In general, the trajectories of the charged particles can be measured through mapping plume characteristics and modeled to follow the local potential field after the point where space charge dominates. Once the space charge boundary has been found, the initial region can be treated as a source function depending mainly on the propellant physical properties (conductivity, surface tension, etc.) and only slightly on the applied field strength as long as the emission site is stable.

In the ideal case, all the charged particles would be accelerated in a straight line with no beam divergence at all. In reality there is some distribution of current density and momentum as a function of angle with the emission site at the origin. The half-angle of the exhaust beam, θ_h, is defined in terms of a cone that encompasses a certain fraction of the total emitted current, typically 95%. The beam spreading efficiency, η_{spread}, is simply the ratio of the actual thrust produced by an emitter, T_{emit}, to the "linear" ideal thrust without beam spreading, T_{linear},

$$\eta_{spread} = \left(\frac{T_{emit}}{T_{linear}}\right)^2 = \left(f(\theta_h)\right)^2 \approx \left(\cos(\theta_h)\right)^2. \tag{11}$$

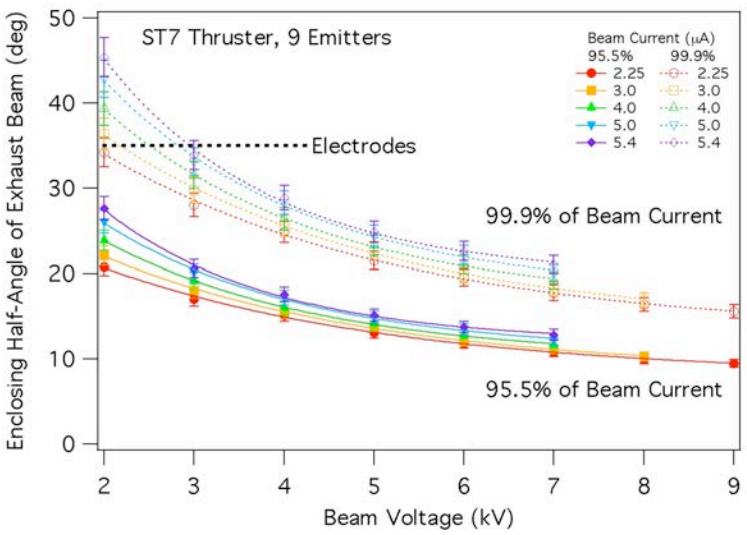

Figure 5. ST7 Colloid thruster exhaust beam profiles with data taken from Demmons, Ref. 10. For normal operating conditions near 6 kV, the half-angle for 95% of the beam current is <15°.

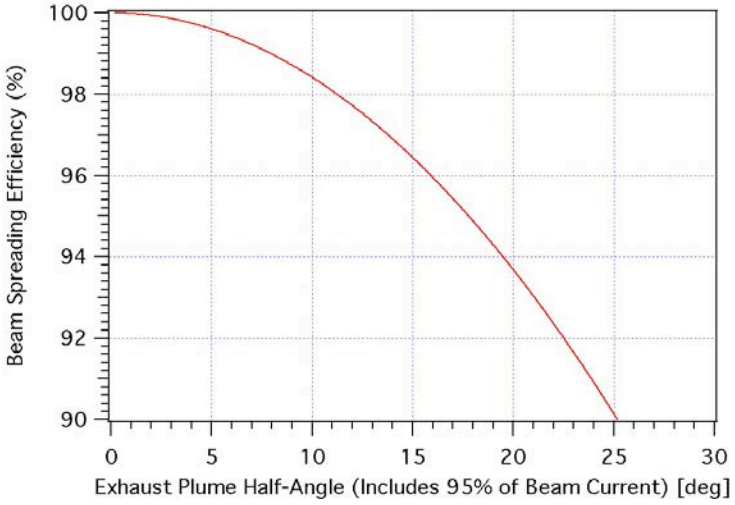

Figure 6. Beam spreading efficiency as a function of exhaust plume half-angle. For half-angles <15°, the efficiency is >96%.

For many exhaust beam distributions, the spreading efficiency can be approximated by the cosine of the half-angle. To determine this efficiency exactly, the exhaust beam profile must be measured including charge and mass flux as a function of angle. Note that, in general, as the current per emitter increases, this efficiency drops, pointing towards lower-current operation per emission sight as the best performance choice.

Plume measurements have been made for a variety of thrusters. In Figure 5 we show exhaust beam profile measurements from the ST7 colloid thruster (with data points taken from Ref. 10 and processed by the author) as a function of beam voltage and total current for 9 emitters. As expected, the beam divergence increases with total current, and increases with decreasing beam voltage. In Figure 6 we show the beam spreading efficiency for the colloid thruster as a function of exhaust beam half-angle. Note that for nominal operation at 6 kV, the beam spreading efficiency is >96%. Once again, this points towards higher voltage operation as being more beneficial from the focusing effects on the exhaust beam.

6. Charge-to-Mass Ratio Efficiency

The final efficiency term is related to the electrospray producing a distribution of charge-to-mass ratios. Since particles with different charge-to-mass ratios will be accelerated to different velocities, there is inefficiency. The mass-averaged exhaust velocity, $\overline{u}_e$, depends on the velocity linearly, while the energy scales as the exhaust velocity squared. Having lighter particles creates only a slightly higher average exhaust velocity while taking significantly more energy. An electrospray producing more than one species will have a lower efficiency than one that produces only ions or droplets with a narrow charge-to-mass distribution. This will be discussed in more detail in the next subsections. For now we define the charge-to-mass ratio distribution efficiency, $\eta_{q/m}$ as,

$$\eta_{q/m} = \left(\frac{\overline{u}_e}{u_{ex}}\right)^2 = \frac{T^2}{2N^2 I_{emit}^2 \left(f(\theta_h)\right)^2 \langle m/q \rangle (V_{beam} - V_{tc})}, \tag{12}$$

where the mass-averaged exhaust velocity and the expected exhaust velocity, u_{ex}, is,

$$\overline{u}_e \equiv \frac{T}{N\dot{m}_n} \quad \text{and} \quad u_{ex} \equiv f(\theta_h)\sqrt{2\left\langle \frac{q}{m} \right\rangle (V_{beam} - V_{tc})} \tag{13a,b}$$

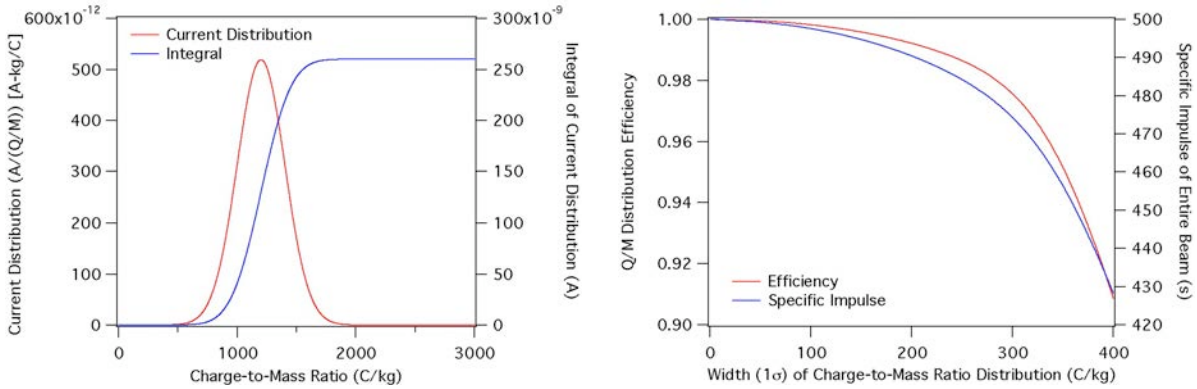

Figure 7. Example of predominantly droplet-mode charge-to-mass ratio distribution in the exhaust of a colloid thruster. As the width of the distribution becomes larger, the impact to the efficient and specific impulse becomes more obvious.

All of these parameters can be measured directly. This efficiency approaches unity only when the electrospray produces a single species with one charge-to-mass ratio. Figure 7 shows an example of a charge-to-mass ratio distribution and its impact on the efficiency and specific impulse. While the average charge-to-mass ratio doesn't change, as the width of the distribution grows, the efficiency and specific impulse begin to drop more severely. Still, with distribution widths <250 C/kg, the distribution efficiency is still >98% for this droplet mode case.

Note that multiplying Eqs. (7-12) together yields Eq. (6). Also note that we can now define useful thrust and specific impulse, I_{sp}, relations,

$$T = \sqrt{\eta_{curr}\eta_{grid}\eta_{spread}\eta_{q/m}} \cdot I\sqrt{2\left\langle\frac{m}{q}\right\rangle\left(V_{beam}-V_{tc}\right)} = C_{eff}I\sqrt{2\left\langle\frac{m}{q}\right\rangle\left(V_{beam}-V_{tc}\right)} \tag{14}$$

$$I_{sp} = \frac{T}{\dot{m}g_0} = \eta_{util}\sqrt{\eta_{grid}}\cdot\frac{\bar{u}_e}{g_0} \tag{15}$$

where C_{eff} is the thrust efficiency coefficient. Note that the thrust does not depend on the mass utilization efficiency, while the specific impulse does linearly.

B. Droplet Mode

A great deal of research has been conducted with electrosprays operating in droplet mode. Fernandez de la Mora has shown with an extensive set of electrospray test data using a variety of liquids [11] that the mass flow rate and square of the current are related by a single parameter. For our analysis, we will use α as the colloid performance parameter, defined by Fernandez de la Mora as follows,

$$\alpha \equiv \sqrt{\frac{2}{I_n}\left\langle\frac{m}{q}\right\rangle} = \sqrt{\frac{\rho\kappa}{\left(f(\kappa)\right)^2\sigma\gamma}} \approx f(temp), \tag{16}$$

where ρ is the density, κ is the dielectric constant, σ is the conductivity, γ is the surface tension, and $f(\kappa)$ is a function dependant only on the dielectric constant that Fernandez de la Mora presented graphically in Ref. 11. Values for the physical properties of EMI-Im have been found in the literature and are plotted in Figure 8 along with the calculated α parameter as a function of temperature using Eq. (16). Note that the conductivity increases by more than a factor of ten over the 100C span from -15 to 85C, which leads to the α parameter changing by a factor of five. The Fernandez de la Mora function for the dielectric constant of EMI-Im is between 7-8 and linearly increases with the dielectric constant. Demmons has measured this colloid performance parameter for EMI-Im directly at three temperatures from 10-30C in Ref. 10 by setting a temperature-controlled electrospray to run at a constant mass flow rate and current. The current was measured by an electrometer during the entire test, and the mass of the propellant

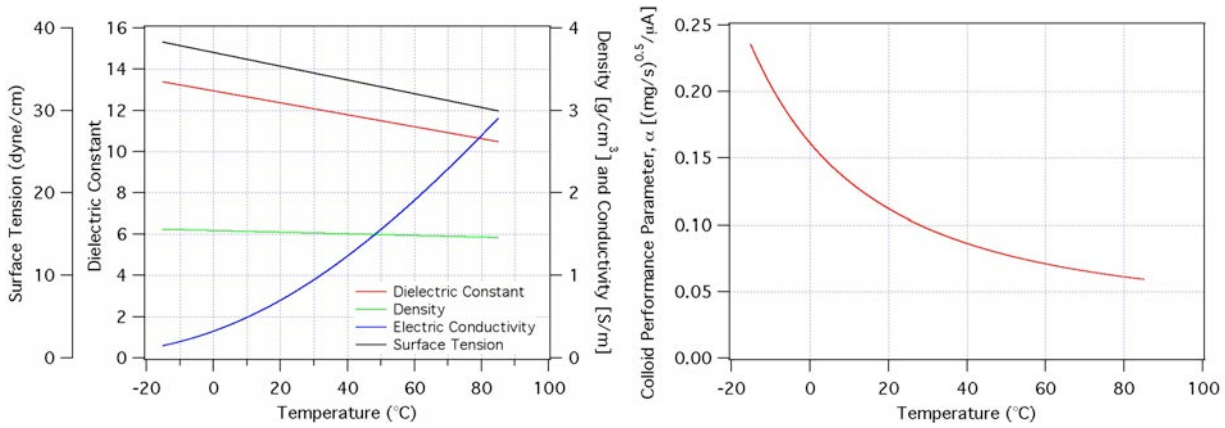

Figure 8. Graphs of the physical properties of EMI-Im as a function of temperature (left) and the corresponding value of α as a function of temperature based on Eq. (16). This parameter as a function of temperature is unique for each electrospray propellant.

reservoir was measured before and after the test to determine the average mass flow rate. The results agree with the calculated version of α within just a few percent over the full 10-30C range [10].

Equation (16) can be re-written in a more useful form along with Eq.(14):

$$\dot{m}_n = \frac{\alpha^2}{2} I_n^2; \left\langle \frac{m}{q} \right\rangle = \alpha^2 \frac{I_n}{2}, \tag{17a,b}$$

$$T = C_{eff} I \sqrt{\alpha^2 \eta_{curr} \frac{I}{N} \left(V_{beam} - V_{tc}\right)} = \left(\frac{\alpha\, C_{eff} \sqrt{\eta_{curr}}}{\sqrt{N}} \right) I^{3/2} \sqrt{\left(V_{beam} - V_{tc}\right)} \tag{18}$$
$$= C_1 I^{3/2} \sqrt{\left(V_{beam} - V_{tc}\right)}$$

$$C_1 = \frac{\alpha}{\sqrt{N}} \eta_{curr} \sqrt{\eta_{grid} \eta_{spread} \eta_{q/m}}\,. \tag{19}$$

Equation (18) provides the functional form for predicting thrust generated in droplet mode based on current and voltage settings or measurements. Since the α parameter is known as a function of temperature and the number of emitters is fixed, evaluating C_1 can be done by estimating the various efficiencies and verified by direct thrust measurements. This is described in Section IV-A for a colloid thruster operating in droplet mode.

C. Ion Mode

When only singly charged ions are being emitted, the charge-to-mass ratio is fixed and Eq. (14) provides the functional form to predict thrust based on the operating current and voltage. The charge should simply be replaced with a unit charge, and the mass should be set appropriate to the molecular weight of the ion. Like Eq. (18) this relation can be evaluated by estimating the various efficiencies and verified by direct thrust measurements. This is described in Section IV-B for a FEEP thruster operating in ion emission mode.

IV. Performance Measurements and Model Validation

A. Colloid Thruster Operating in Droplet Mode

The thrust produced by a colloid thruster designed for precision drag-free applications is difficult to measure. On the order of 10 μN, the thrust-to-weight ratio of these devices can easily be 10^{-6}. Both Gamero [12] and Roy [13] have completed these measurements at Busek Co. using a six-emitter thruster and a nine-emitter thruster, respectively, both operating near room temperature. We have decided to use Roy's results here as the author assisted in their acquisition, and we are familiar with the results.

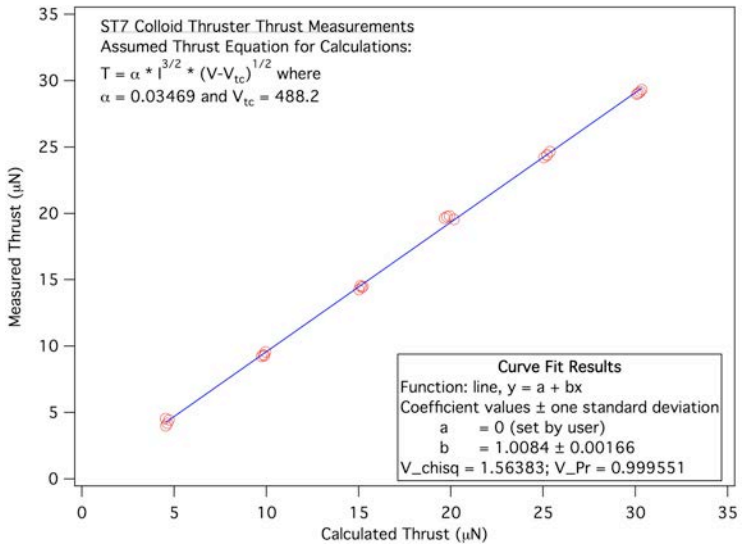

Figure 9. Measured vs. Calculated Thrust based on Eq. (18) and the parameters shown in the plot. Data taken from Roy, Ref. 13.

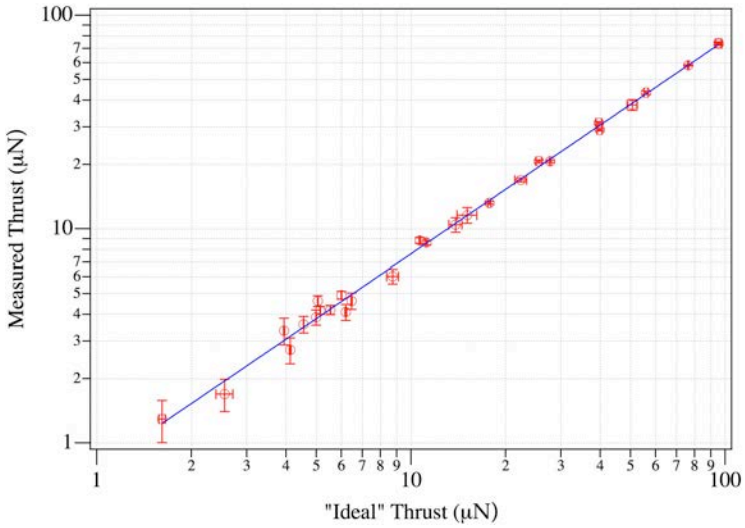

Figure 10. InFEEP Measured Thrust vs. "Ideal" Thrust from Eq. (14). Plot taken from Ziemer, Ref. 14.

The thrust stand measurements were conducted as follows: for six different conditions, a current and voltage was set based on predictions to produce 5, 10, 15, 20, 25, and 30 μN, spanning between 2 – 10 kV and 2 – 5 μA. Each trial was repeated at least three times over a week of testing. The Busek thrust stand has a resolution of approximately 50 nN and an accuracy to within about 2% [13]. For this analysis the "calculated thrust" was determined using Eq. (18) assuming a C_{eff} of 0.97, an α of 0.11 (See Figure 8 at 25C) and compared to the measured thrust to determine V_{tc} with the best linear fit. The results are shown in Figure 9, showing very good agreement with the performance model using a linear fit between the calculated thrust and the measured thrust. Note that the best fit to the V_{tc} parameter is ~500V, which is also in good agreement with the retarding potential measurements shown in Figure 4. This indicates that the efficiencies going in the thrust coefficient, C_1, are all near unity for the ST7 colloid thruster.

B. Needle-FEEP Operating in Ion Mode

Thrust measurements of the InFEEP with a single needle emitter taken by this author in 2001 [14] using the JPL Sub-Micronewton Thrust Stand (~0.1 μN resolution with better than 2% accuracy). With only one extractor/accelerator electrode besides the emitter and a passive feed system, changing the applied voltage, which then also determined the beam current, was used to vary thrust. In this case the "ideal" thrust was calculated from the performance model in Eq. (14) with C_{eff} set to 1 and V_{tc} set to 0 V. A linear fit between the ideal and measured thrust show that the ion emission model works well, assuming the C_{eff} should be set to 0.7 to 0.8. Note that the propellant utilization efficiency shown in Figure 3 for the InFEEP does not show up in the thrust performance relation or in the thrust measurements. The two inefficiencies that are the most significant are the grid and spread efficiencies with as much as 20% of the beam current intercepted by the extractor electrode and half-angles as high as 50° leading to spreading efficiencies between 60-75%. Fortunately the highest beam currents are produced at the highest beam voltages, which help to offset each other. More recent designs of the InFEEP thruster include focusing electrodes that significantly reduce grid impingement and beam spreading.

V. Conclusion

Electrospray thrusters have the potential to rival and even surpass more developed ion and Hall thrusters in terms of system-level performance. There are many types and configurations that can be useful, but it's clear that more research work needs to be done to determine the best approaches. This paper provides the framework for evaluating options using verified performance models.

If these devices can be successfully scaled from the micronewton to millinewton thrust levels, they may become appropriate as the primary propulsion for power limited, small-sat missions. Scaled to even larger thrust and power levels, arrays of electrospray emitters could compete with the system-level performance of conventional Hall and ion thrusters. At the system level, having multiple liquid or solid propellants to chose from compared to relatively few conveniently stored gas propellants also has its advantages, including the ability to use one propellant for both high and low thrust maneuvers very efficiently (dual-mode operation). However, many challenges exist with both the single-emitter and multi-emitter configurations related to the nature of the propellant, feed system and propellant delivery, and the typically small dimensions of these devices. There are many trade-offs between performance and ease of manufacturing as well as reliability. While we only touched on some of these challenges in this paper, the focus was on motivating the future development of electrospray propulsion devices by presenting verified performance scaling relationships.

Acknowledgments

The author would like to thank Tom Roy and Nathaniel Demmons from Busek Co. for the use of their thrust stand data and beam profile measurements.

The research work described in this paper was carried out at the Jet Propulsion Laboratory, California Institute of Technology, under a contract with the National Aeronautics and Space Administration. Reference herein to any specific commercial product, process, or service by trade name, trademark, manufacturer, or otherwise, does not constitute or imply its endorsement by the United States Government or the Jet Propulsion Laboratory, California Institute of Technology.

References

[1]Martinez-Sanchez, M., Fernandez de la Mora, J., Hruby, V., Gamero-Castaño, M., and Khayms, V., "Research on Colloid Thrusters," *Proceedings of the 26th International Electric Propulsion Conference*, Kitakyushu, Japan, Oct. 1999, IEPC-99-014.

[2]Mitterauer, J., "Liquid-Metal Ion Sources as Thrusters for Electric Space Propulsion," *Journal de Physique*, Vol. 48, No. C-6, Nov. 1987, pp171-176.

[3]Gamero-Castaño, M. and Hruby, V., "Electrospray as a Source of Nanoparticles for Efficient Colloid Thrusters," *AIAA J. of Prop Power*, Vol . 17, No. 5, September– October, 2001.

[4]Hruby, V., et al, "ST7-DRS Colloid Thruster System Development and Performance Summary," *Proceedings of the 44th AIAA Joint Propulsion Conference*, Hartford, CT, July 21-23, 2008. AIAA-2008-4824.

[5]Ziemer, J.K., et al, "Delivery of Colloid Micro-Newton Thrusters for the Space Technology 7 Mission," *Proceedings of the 44th AIAA Joint Propulsion Conference*, Hartford, CT, July 21-23, 2008. AIAA-2008-4826.

[6]Nicolini, D., "LISA Pathfinder Field Emission Thruster System Development Program," *Proceedings of the 30th International Electric Propulsion Conference*, Florence, Italy, 2007, IEPC-2007-363.

[7]Marrese-Reading, C., "In-FEEP Thruster Ion Beam Neutralization with Thermionic and Field Emission Cathodes," *Proceedings of the 27th International Electric Propulsion Conference*, Pasadena, California Oct. 2001, IEPC-2001-290.

[8]Tajmar, M., Genovese, A., and Steiger, W., "Indium Field Emission Electric Propulsion Microthruster Experimental Characterization," *AIAA J. of Prop Power*, Vol . 20, No. 2, March-April, 2004.

[9]Gamero-Castaño, M., "Characterization of the electrosprays of 1-ethyl-3-methylimidazolium bi(trifluoromethylsulfonyl) imide in vacuum," Physics of Fluids, Vol. 20, No. 032103, 2008.

[10]Demmons, N., et al, "ST7-DRS Mission Colloid Thruster Development," *Proceedings of the 44th AIAA Joint Propulsion Conference*, Hartford, CT, July 21-23, 2008. AIAA-2008-4823.

[11]Fernandez de la Mora, J. and Loscertales, I.G., "The Current Emitted by Highly Conducting Taylor Cones," *J of Fluid Mech*, Vol. 260, Feb. 1994, pp. 155-184.

[12]Gamero-Castaño, M., "Characterization of a Six-Emitter Colloid Thruster Using a Torsional Balance," *AIAA J. of Prop Power*, Vol . 20, No. 4, July-August, 2004.

[13]Roy, T., Ziemer, J.K., et al, "Direct Thrust Measurements of the NASA ST7 Colloid Micro-Newton Thruster", *JANNAF Space Propulsion Subcommittee Meeting Proceedings*, Orlando, Florida, December 2008. Tracking Number SPS-III-21.

[14]Ziemer, J.K., "Performance Measurements Using a Sub-Micronewton Resolution Thrust Stand," *Proceedings of the 27th International Electric Propulsion Conference*, Pasadena, California Oct. 2001, IEPC-2001-238.